GEPP-TIS-495

STRESS ANALYSIS OF GLASS-CERAMIC INSULATOR AND MOLYBDENUM CYLINDERS IN VACUUM TUBE SUBASSEMBLY

R. K. Spears
Metallurgy & Ceramics Laboratory

June 10, 1980

General Electric Company
Neutron Devices Department
P. O. Box 11508
St. Petersburg, Florida 33733

Prepared for the
U. S. Department of Energy
Albuquerque Operations Office
Under Contract No. DE-AC04-76DP00656

Printed in the United States of America
Available from
National Technical Information Service
U.S. Department of Commerce
5285 Port Royal Road
Springfield, VA 22161
Price: Printed Copy $ 4.50 ;Microfiche $2.25

ABSTRACT

This study determined the state of stress between molybdenum cylinders and a glass-ceramic insulator of a vacuum tube during cooling when the glass-ceramic coefficient of expansion differed from molybdenum by $\pm 2 \times 10^{-7}/^{o}C$. A thermoelastic stress analysis was performed on the vacuum tube subassembly using the finite element method. Two cases, which examined the effect of cooling over a 700°C range, were considered. In Case One, the expansion coefficient of the glass-ceramic was $2 \times 10^{-7}/^{o}C$ less than that of molybdenum while for Case Two, it was $2 \times 10^{-7}/^{o}C$ greater. For Case One, it was found that the tangential stresses in the insulator were entirely compressive but the maximum principal stresses in the r-z plane were mainly tensile. For Case Two, the tangential stresses were tensile in the insulator as were most of the maximum principal stresses in the r-z plane except for stress in the upper regions of the insulator. The magnitude of the stress at the maximum principal stress location appears to be substantially lower than what has been observed in practice (i.e., cracking of this design had never been a major problem, but it has been observed that if the coefficient of expansion of the glass-ceramic was $2 \times 10^{-7}/^{o}C$ lower than molybdenum, cracking usually resulted). This analysis showed that the expansion coefficient of the glass-ceramic could be varied quite liberally from molybdenum before the ultimate strength (13,000 lb/in.^{2}) of the glass-ceramic was exceeded.

CONTENTS

ILLUSTRATIONS

ILLUSTRATIONS

TABLES

INTRODUCTION

A vacuum tube subassembly is fabricated at the General Electric Neutron Devices Department (GEND) by bonding a glass-ceramic insulator between two molybdenum cylinders (Figure 1) at an elevated temperature. Since both the glass-ceramic and molybdenum are quite brittle, it is desirable that their coefficients of expansion be matched to minimize residual stresses. This is especially critical during the cooling cycle from the glass-ceramic set point to room temperature. Due to compositional differences from batch to batch, glass-ceramics having slightly different expansions are expected. Because of the difficulty in assessing the state of stress based on an intuitive approach, a theoretical analytical stress analysis was performed. This analysis will also act as a guide in an experimental stress analysis using X-ray diffraction.

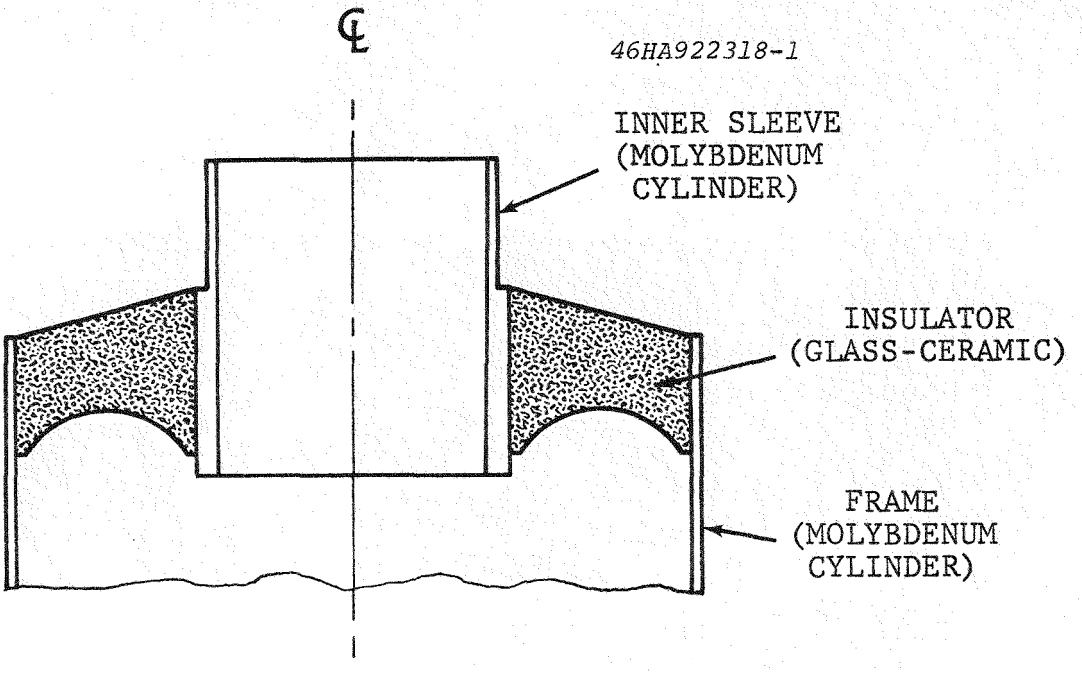

Figure 1. Vacuum Tube Envelope Subassembly

METHOD OF ANALYSIS AND CONFIGURATION

Stress was analyzed using a finite element code for elastic materials and axisymetric structures. The r-z plane of the subassembly configuration is shown in Figure 2.

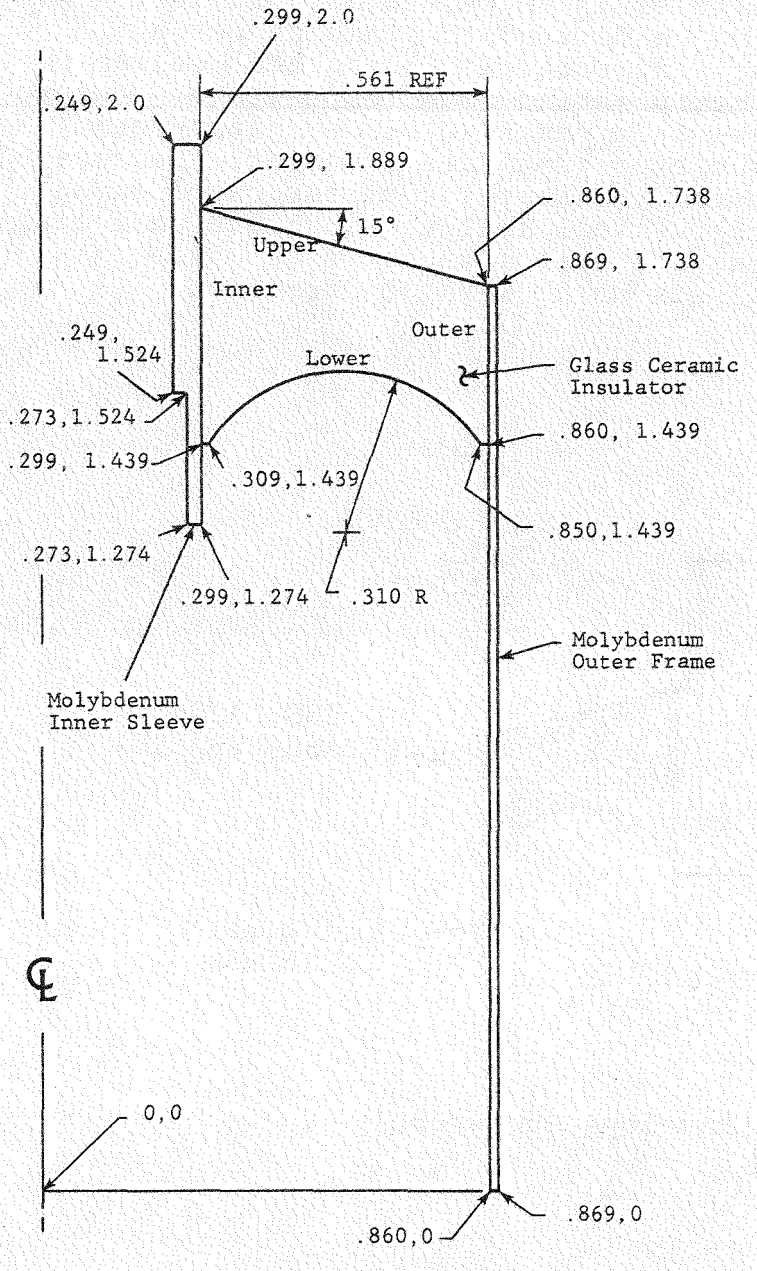

Figure 2. The r-z Plane of Vacuum Tube Envelope Subassembly (Dimensions in Inches)

The mesh geometry, which uses 313 nodal points and 262 elements, is shown in the Appendix (Figure 1-A). The material properties are shown in Table 1. For this study a temperature interval of 700°C, corresponding to a decrease in temperature from the glass-ceramic set point (725°C) to room temperature (25°C), was used.

Table 1. Properties of Molybdenum and Glass-Ceramic Used in Analysis

	Elasticity Modulus (E) ($lb/in.^2$)	Poisson Ratio (ν)	Coefficient of Expansion (α)
Molybdenum	47×10^6	0.30	$55 \times 10^{-7}/°C$
Glass-Ceramic	11.7×10^6	0.26	Case One, $53 \times 10^{-7}/°C$ Case Two, $57 \times 10^{-7}/°C$

Both recrystallized molybdenum and the glass-ceramic are considered brittle materials and exhibit little or no plastic deformation before ultimate failure. For this reason the failure criteria was based on the maximum principal stress; this was consistent with brittle material yield theories.

The general state of stress for axisymmetric symmetry consists of four independent components: The axial stress (σ_z), the radial stress (σ_r), the tangential or hoop stress (σ_T) and the shear stress in the r-z plane (σ_{rz}). These can be resolved into three principal stresses σ_I, σ_{II}, and σ_{III} (where $\sigma_I > \sigma_{II} > \sigma_{III}$) in which case σ_T is one principal stress while the other two are in the r-z plane. The maximum principal stresses in the r-z plane are designated as $\sigma_{I,rz}$ while the principal stresses in the tangential direction is designated as σ_T.

RESULTS

CASE ONE - WHEN COEFFICIENT OF EXPANSION OF GLASS-CERAMIC IS LESS THAN THAT OF MOLYBDENUM

In this case, because the molybdenum contracts at a greater rate during cool-down than the glass-ceramic, it would appear that the general state of stress would be compression at the outer interface and tensile at the inner interface. For the most part as shown in Figure 3, the maximum principal stresses are tensile in the r-z plane although at the outer interface there is a region of compression. On the other hand, σ_T is entirely compressive throughout the insulator.

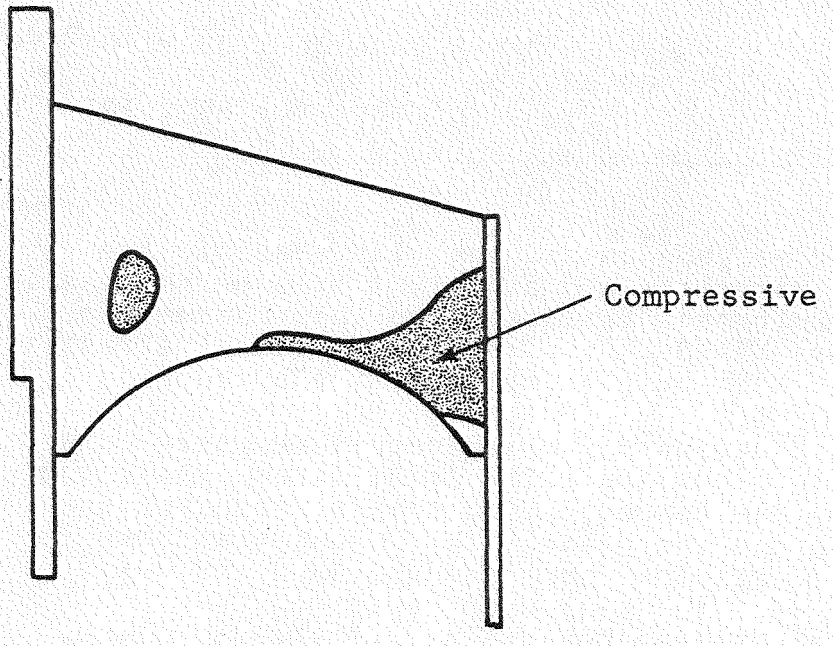

Figure 3. Location of Regions in the r-z Plane in Which the Maximum Principal Stresses are Compressive for Case One

On actual subassembly piece parts where the insulator thermal expansion coefficient was less than molybdenum, Zyglo* adsorption at the top of the outer surface (at the glass-ceramic frame interface) had been observed. The adsorption was usually a full 360° and was generally attributed to tensile radial stresses in that area. These radial stresses appear to be caused in part by the manner in which the outer frame is restrained by the glass-ceramic during cool-down. This is illustrated in Figure 4, Part A, which is a plot of the room temperature displacement of the outer molybdenum surface. It appears that a bending moment is created in the outer frame as a result of the restraining effect of the glass-ceramic at the lower portion of the frame-insulator interface. The result is a tensile radial stress in the top interfacial element of the insulator of 378 lb/in.^{2}. This, combined with an axial compressive stress of -520 lb/in.^{2} and an r-z shear stress of -178 lb/in.^{2}, produces a principal stress of 444 lb/in.^{2}.

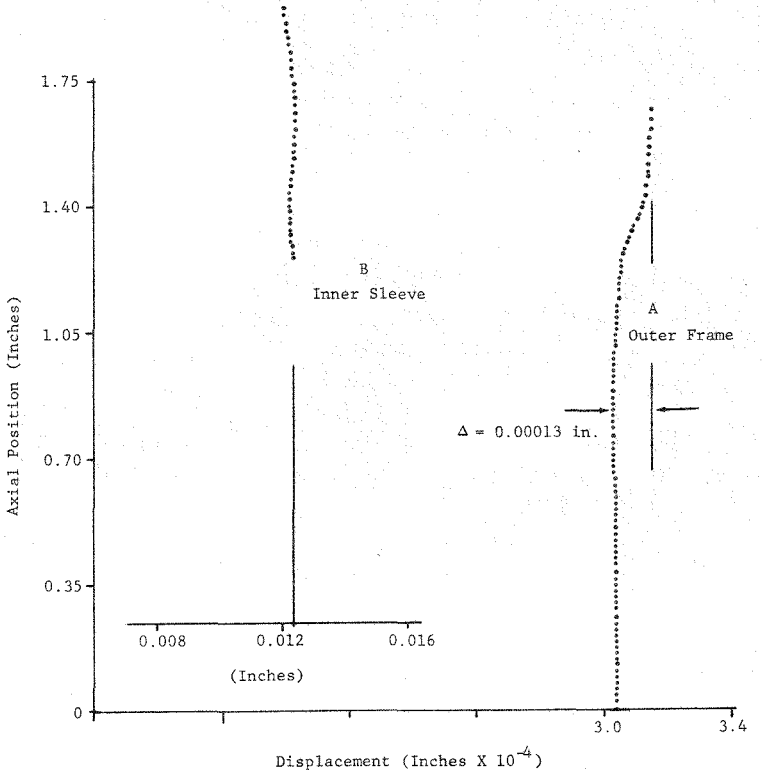

Figure 4. Frame and Inner Sleeve Outer Surface Positions After Sealing. (Part A Shows the Position of the Outer Surface of the Frame While Part B Shows the Position of the Outer Surface of the Inner Sleeve. Case One.)

*Trademark, Magnaflux Corp.

A complete description of the state of stress in the elements in this vicinity is shown in Figure 5.

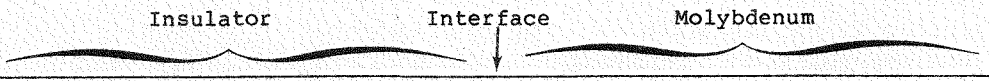

σ_r, element	312	241	455	242	378	243	-131	244	-93	245	-108	246
σ_z	7		106		-520		3816		2965		2436	
$\sigma_{T,rz}$	-68		-33		-178		7140		5837		6643	
$\sigma_{I,rz}$	-340		455		444		4000		3000		2437	
σ_T	-83		-3		-178		7150		6840		6647	
σ_r, element			-187	225	-30	226	-81	221	19	228	45	229
σ_z			21		-638		4445		4150		3790	
$\sigma_{T,rz}$			13		-261		300		30		210	
$\sigma_{I,rz}$			188		65		4465		4170		3800	
σ_T			-132		-371		7074		6980		6850	
σ_r, element					-45	209	4880	210	4730	211	4600	212
σ_z					-671		4880		4590		4600	
$\sigma_{T,rz}$					-445		7040		6980		6290	
$\sigma_{I,rz}$					-45		4880		4730		4600	
σ_T					-445		7045		6980		6920	

Figure 5. An Element-by-Element Listing of the Stresses in Elements Near the Upper Outside Corner of the Assembly (Values in lb/in.^{2})

The reason σ_T is compressive at the inner surface of the insulator is not completely clear. It is believed to be caused by the high shearing stresses and highly compressive axial stresses at the inner surface. Shown in Figure 4, Part B, is the displacement of the outer surface of the inner molybdenum sleeve. Due to the stiffness of this member, the surface displacement is small. However, there is a slight outward bow at the midsection verifying the fact that the contraction of the sleeve is constrained by the glass-ceramic. As expected, σ_T and $\sigma_{I,rz}$ on the outer portion of the inner sleeve are largely tensile at the glass-ceramic interface (Figure 6, Parts A and B).

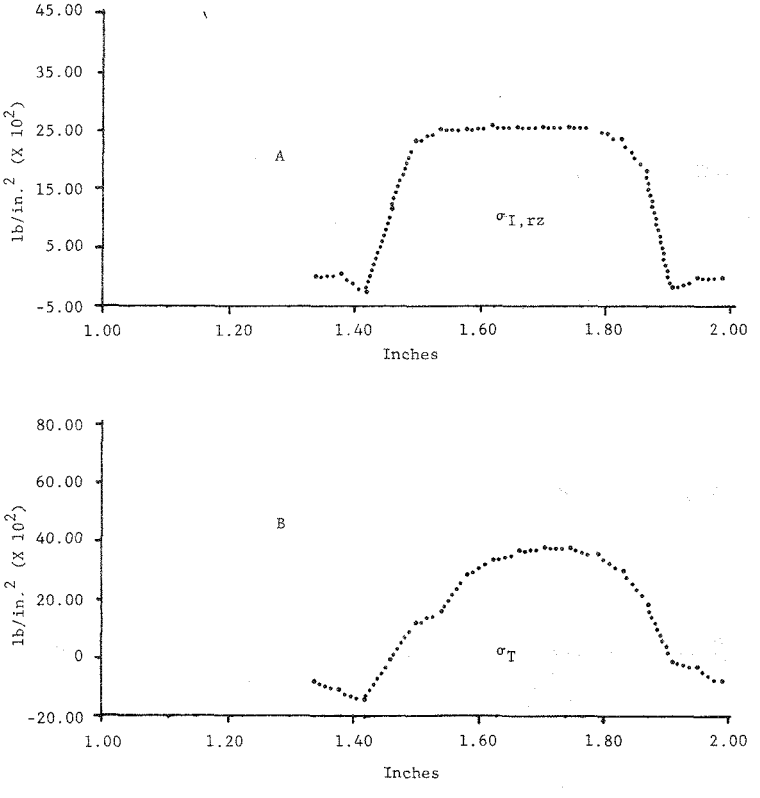

Figure 6. Stresses Mounted on Outside Surface of Sleeve. (Part A Shows the Maximum Principal Stresses While Part B Shows the Tangential Stresses. Case One.)

The stress distribution across the top and bottom surfaces of the insulator are shown in Figures 7 and 8. The location of the maximum principal stress in the insulator is in the top surface 0.38 inch from the axis of the assembly. This stress is in the r-z plane.

For reference purposes, graphs of principal stresses at the lower surface as well as at the inner and outer interfaces are shown in Figures 7, 8, 9, 10 and 11. Figure 12 shows the axial and tangential stresses on the outer molybdenum surface. This will be of importance as reference information in the X-ray diffraction experimental stress analysis. The data from which Figure 12 was obtained is tabulated in the Appendix (Table 1-A). The strain is also tabulated.

CASE TWO - WHEN COEFFICIENT OF EXPANSION OF GLASS-CERAMIC IS GREATER THAN THAT OF MOLYBDENUM

For this condition it might be expected that the general state of stress in the insulator would be compressive at the inner surface and tensile at the outer. As shown in Figure 13, $\sigma_{I,rz}$ stresses are tensile throughout the insulator except along the upper surface. Even though radial stresses at the inner surface of the insulator are compressive, the principal stress $\sigma_{I,rz}$ is tensile because of the tensile axial stress at the interface.

The reason σ_T in the insulator is tensile at the inner surface is not completely understood. Both σ_T and $\sigma_{I,rz}$ on the outer surface of the molybdenum inner sleeve are compressive (Figure 14, Parts A and B).

The stress distribution at the upper and lower surfaces of the insulator are shown in Figures 15 and 16. The location of the maximum principal stress is in the lower surface near the inner sleeve. This is a tangential stress of 1800 lb/in.^{2}.

The displacement of the outer surface of the frame and outer surface of the sleeve is shown in Figure 17.

For reference purposes, stresses at the inner and outer interfaces are plotted in Figures 18, 19, and 20. Figure 21, Parts A and B, which show the axial and tangential stresses and strains in the outer molybdenum frame, are included as reference material for an experimental stress analysis using X-ray diffraction. This data is tabulated in the Appendix (Table A-2).

Text continued on page 16.

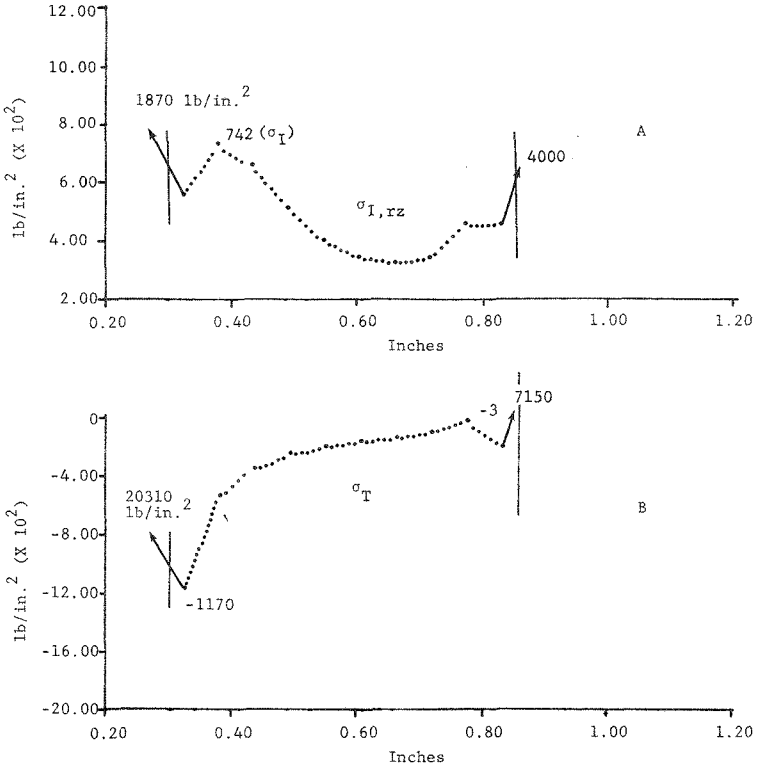

Figure 7. Stresses, Top Surface, Insulator. (Part A Shows the Maximum Principal Stresses While Part B Shows the Tangential Stresses. Case One.)

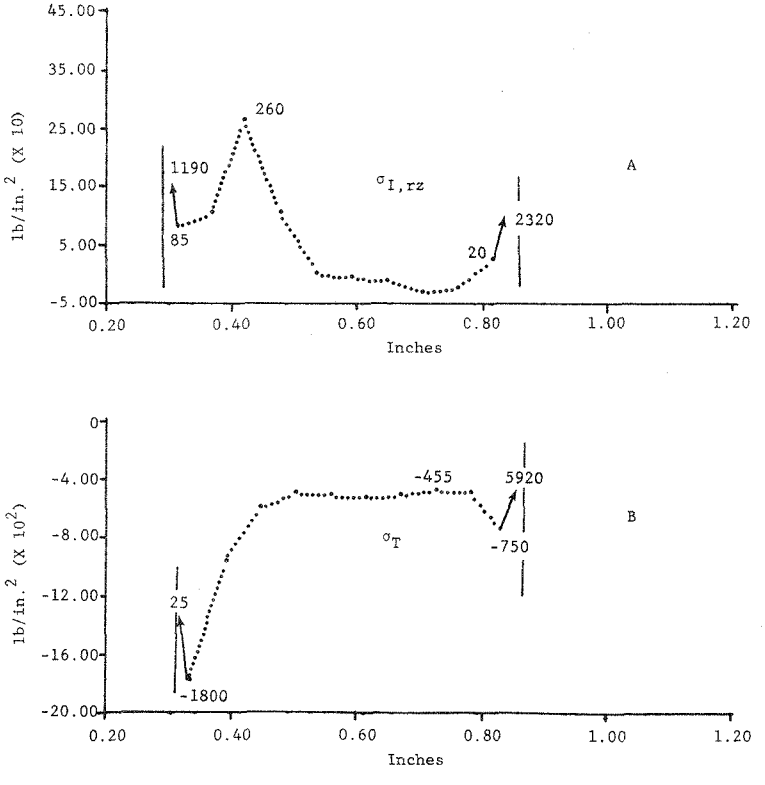

Figure 8. Stresses, Bottom Surface, Insulator. (Part A Shows the Maximum Principal Stresses, While Part B Shows the Tangential Stresses. Case One.)

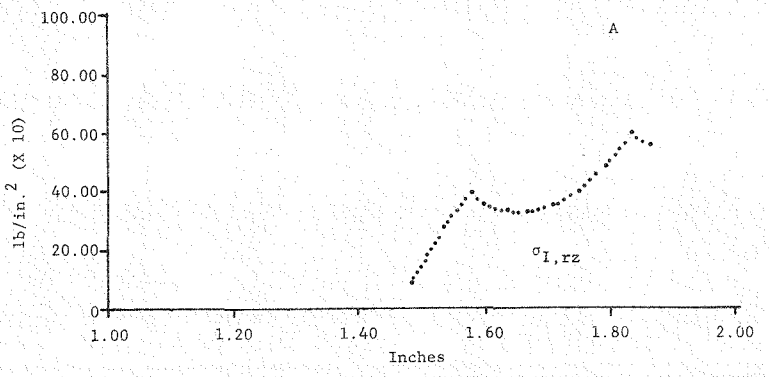

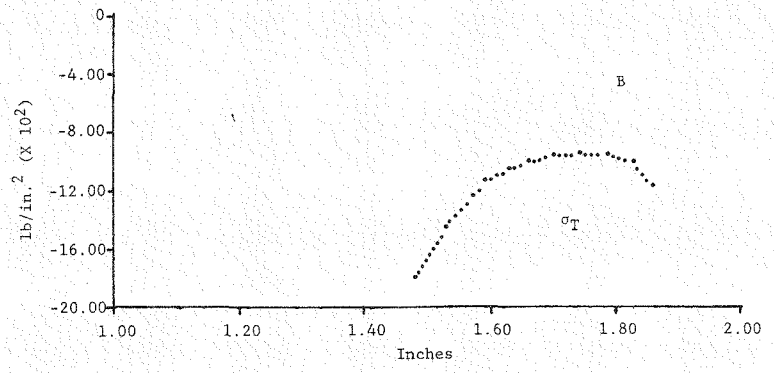

Figure 9. Stresses, Inner Surface, Insulator. (Part A Shows the Maximum Principal Stresses While Part B Shows the Tangential Stresses. Case One.)

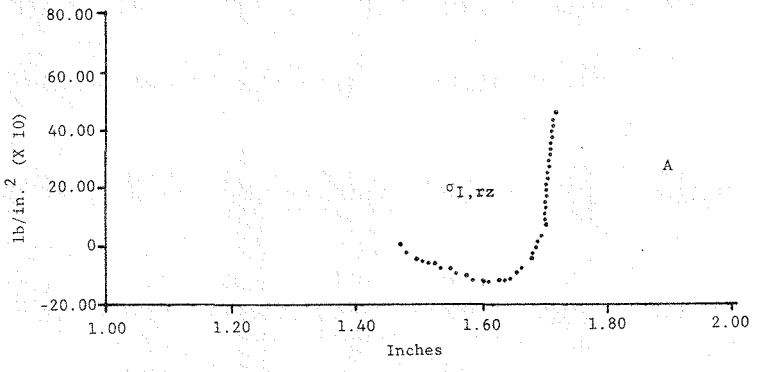

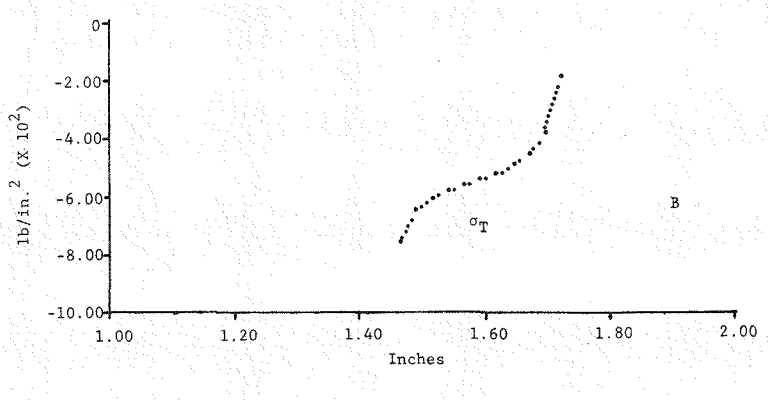

Figure 10. Stresses, Outer Surface Insulator. (Part A Shows the Maximum Principal Stresses, While Part B Shows the Tangential Stresses. Case One.)

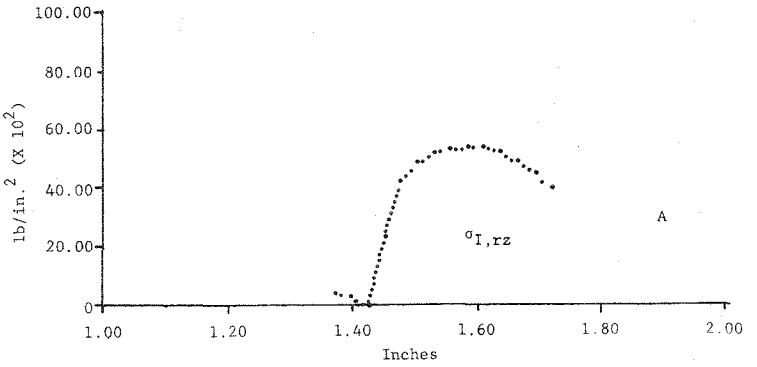

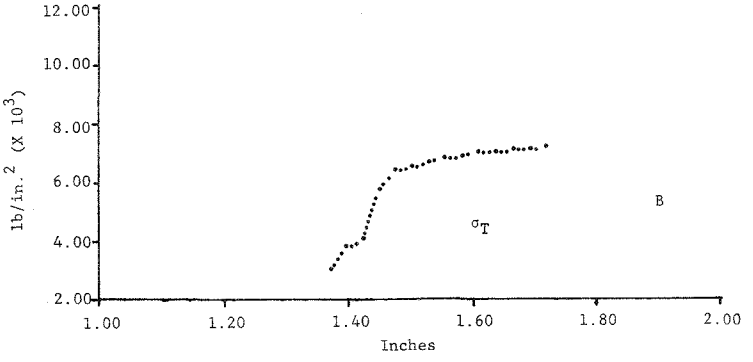

Figure 11. Stresses, Inner Surface, Frame. (Part A Shows the Maximum Stresses While Part B Shows the Tangential Stresses. Case One.)

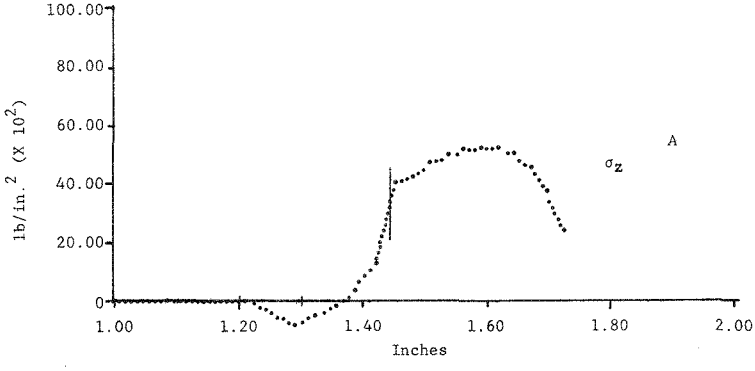

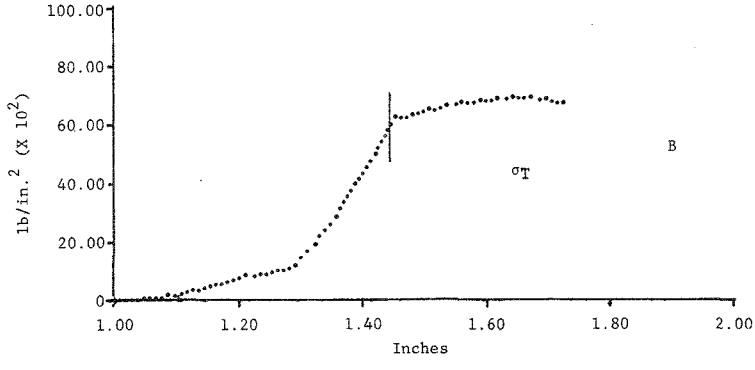

Figure 12. Stresses, Outer Surface, Frame. (Part A Shows the Axial Stresses While Part B Shows the Tangential Stresses. Case One.)

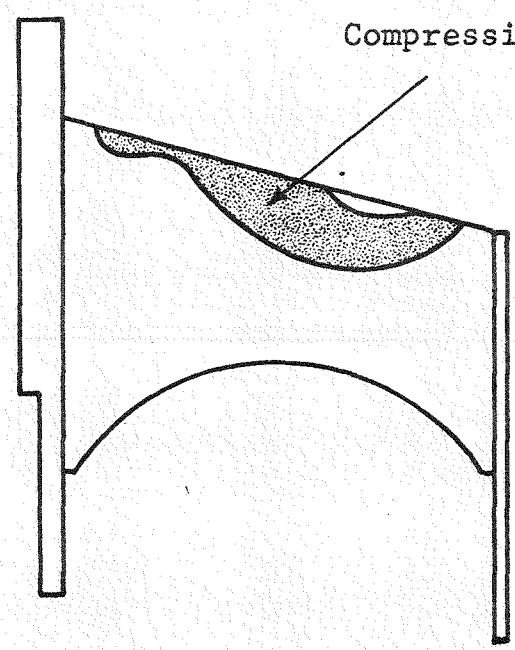

Figure 13. Compressive Stresses, Insulator. (Case Two)

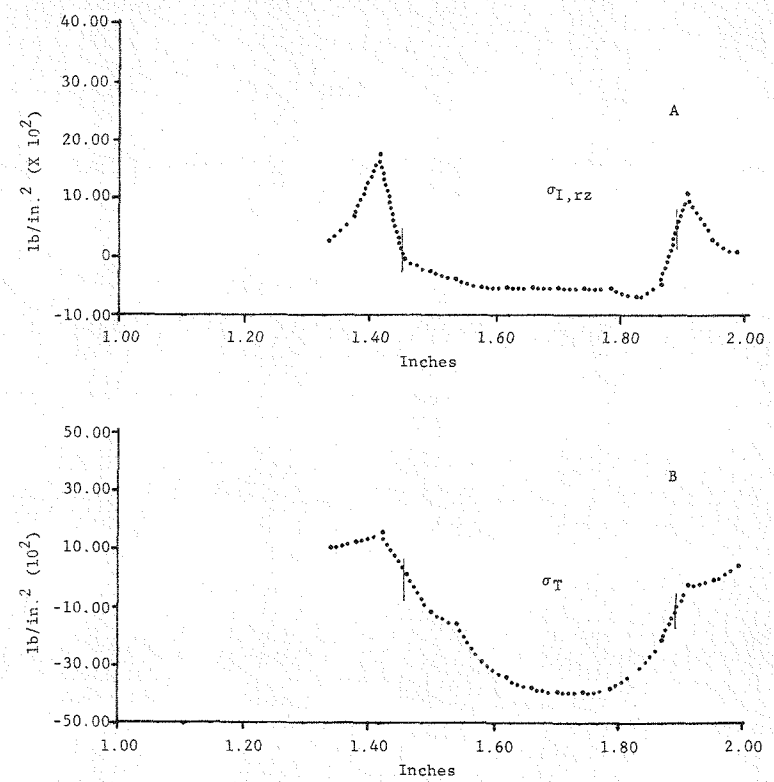

Figure 14. Stresses, Outer Surface, Inner Sleeve. (Part A Shows the Maximum Principal Stresses While Part B Shows the Tangential Stresses. Case Two. α G.C. > α Molybdenum.)

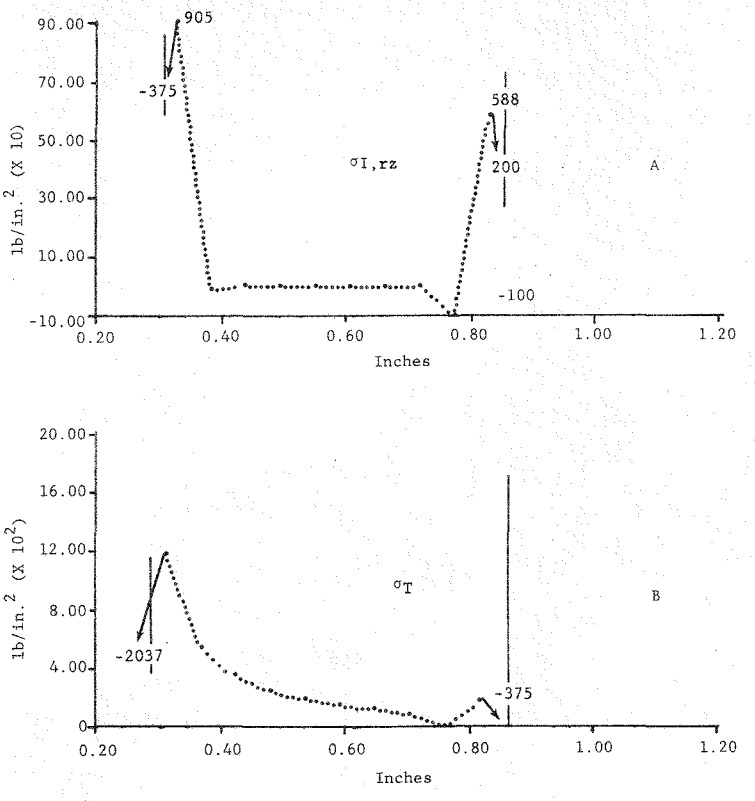

Figure 15. Stresses, Top Surface, Insulator. (Part A Shows the Maximum Principal Stresses While Part B Shows the Tangential Stresses. α G.C. > α Molybdenum. Case Two.)

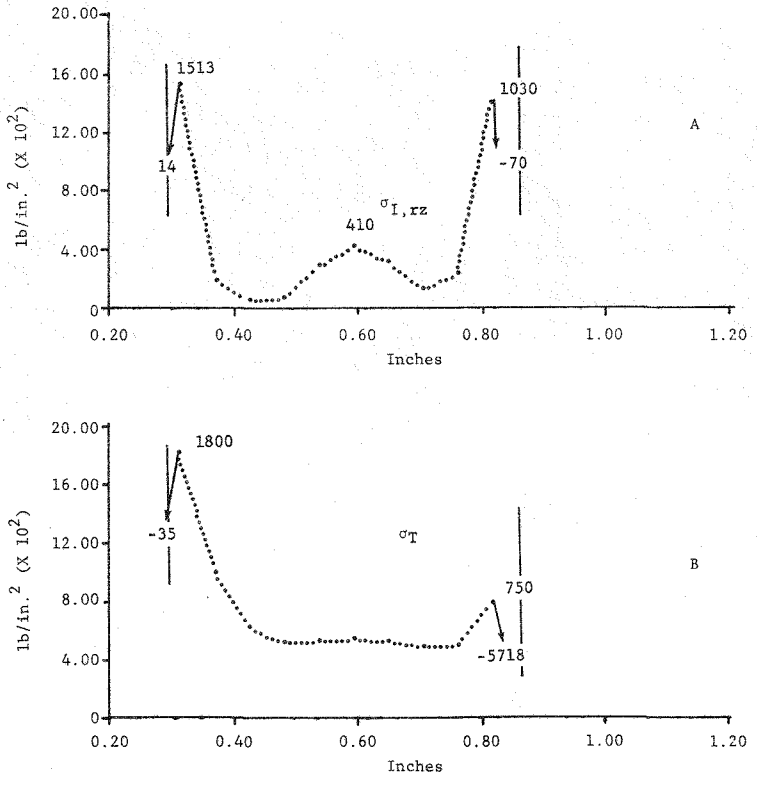

Figure 16. Stresses, Bottom Surface, Insulator. (Part A Shows the Maximum Principal Stresses While Part B Shows the Tangential Stresses. α G.C. > α Molybdenum. Case Two.)

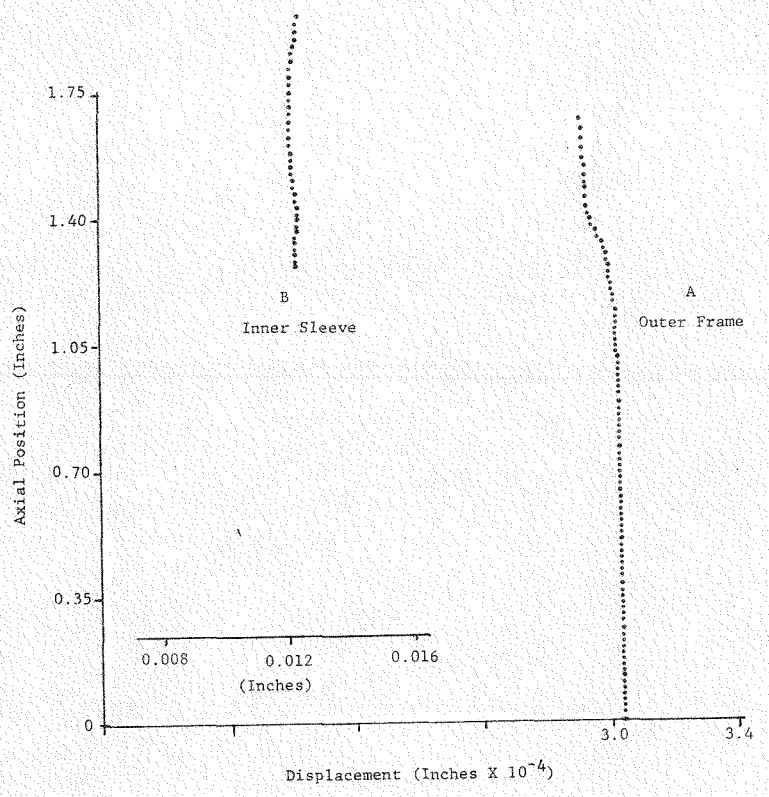

Figure 17. Frame Outer Edge and Sleeve Inner Surface Position After Sealing. (Part A Shows the Position of the Outer Edge of the Frame While Part B Shows the Position of the Inner Surface of the Sleeve. Case Two.)

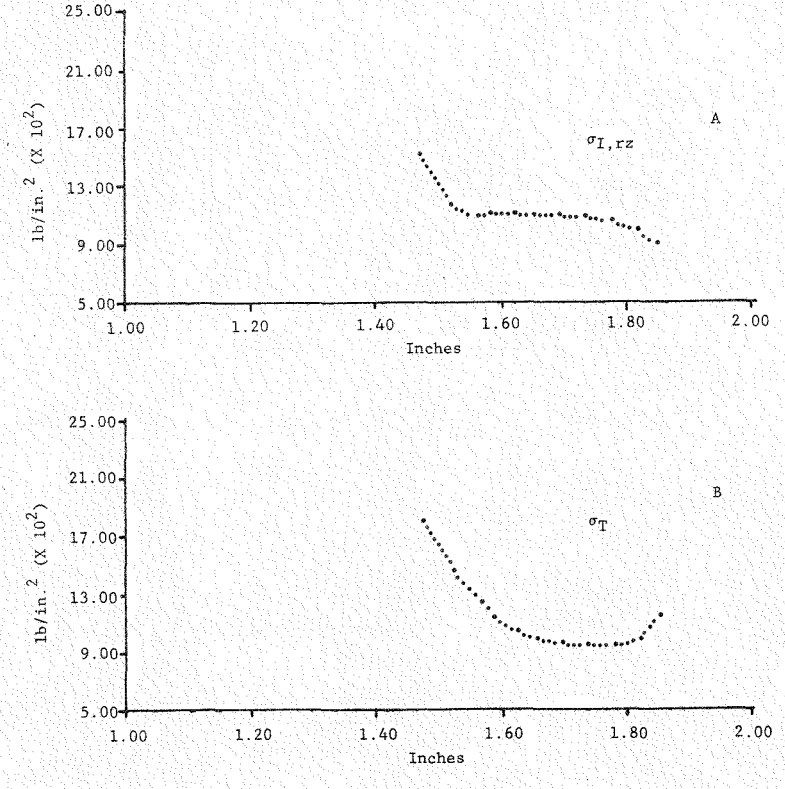

Figure 18. Stresses, Inner Surface, Interface. (Part A Shows the Maximum Principal Stresses, at the Inner Surface, While Part B Shows the Tangential Stresses. α G.C. > α Molybdenum. Case Two.)

Figure 19. Stresses, Outer Surface, Insulator. (Part A Shows the Maximum Principal While Part B Shows the Tangential Stresses. α G.C. > α Molybdenum. Case Two.)

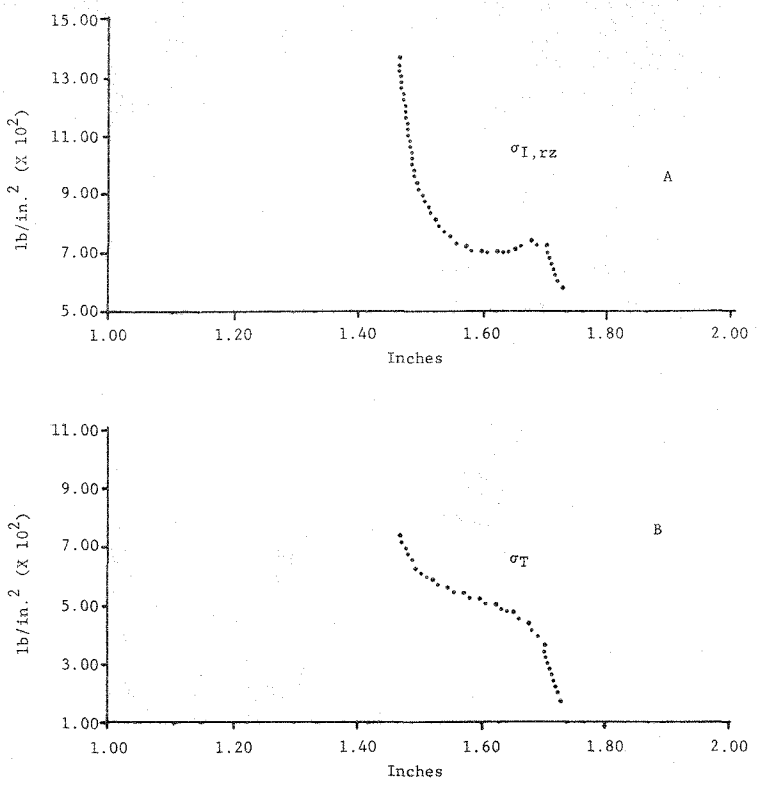

Figure 20. Stresses, Inner Surface, Frame. (Part A Shows the Maximum Stresses While Part B Shows the Tangential Stresses. α G.C. > α Molybdenum. Case Two.)

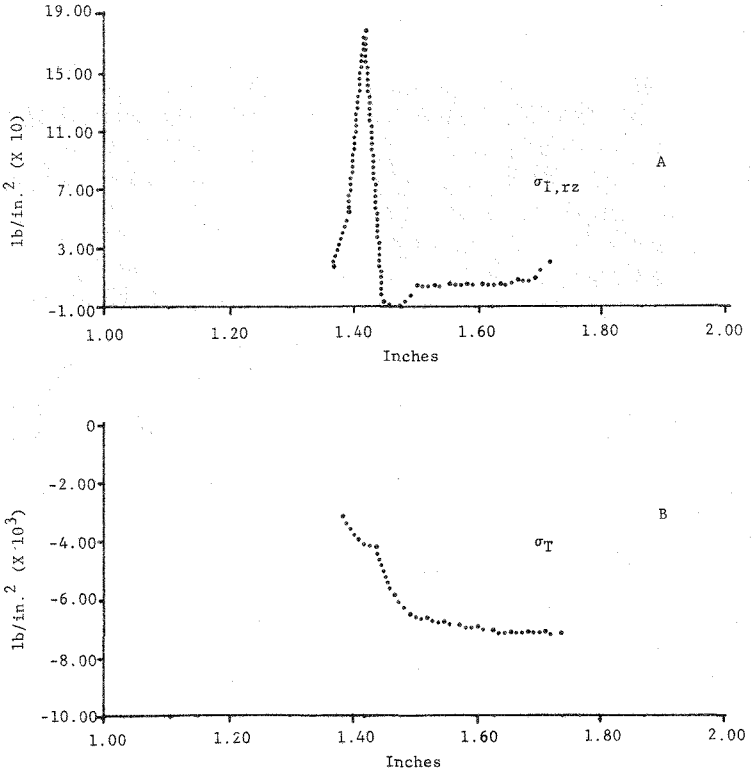

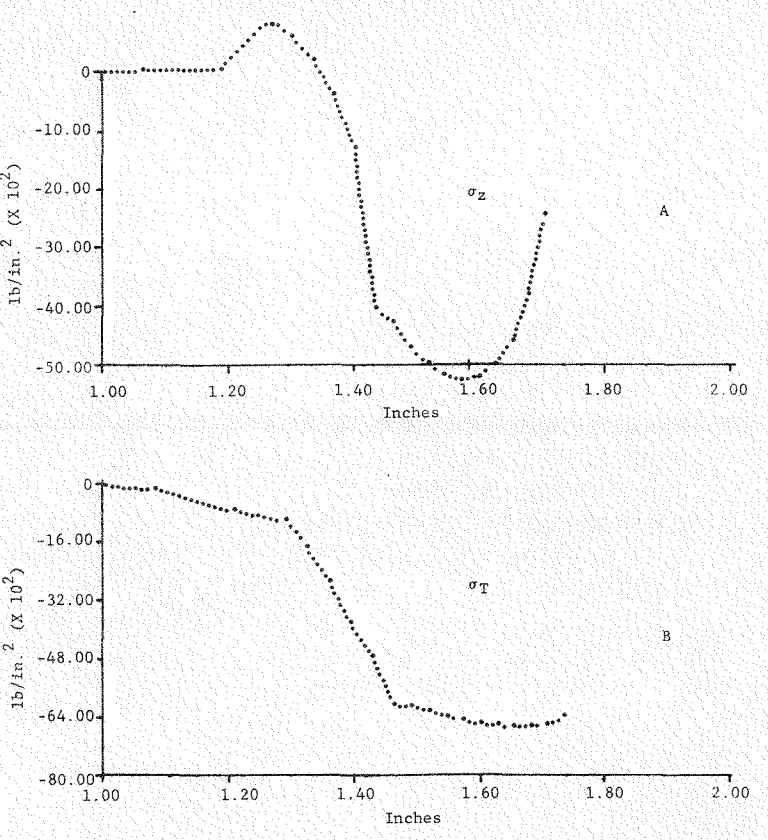

Figure 21. Stresses, Outer Surface, Frame. (Part A Shows the Axial Stresses, While Part B Shows the Tangential Stresses. α G.C. > α Molybdenum. Case Two.)

DISCUSSION

Using the results of these studies it was intended to predict the expansion difference necessary to fracture the glass-ceramic. The ultimate tensile strength of the glass-ceramic is 13,000 lb/in.^{2}. For Case One, where the glass-ceramic expansion was less than molybdenum, the analysis showed that the expansion can be as much as 35 x $10^{-7}/^{o}C$ below molybdenum, while for Case Two, where the glass-ceramic expansion was greater than molybdenum, the analysis showed that the expansion of the glass-ceramic can be as much as 14 x $10^{-7}/^{o}C$ above the expansion of the molybdenum. A summary of the results of this analysis showing maximum stresses versus expansion differences is shown in Figure 22.

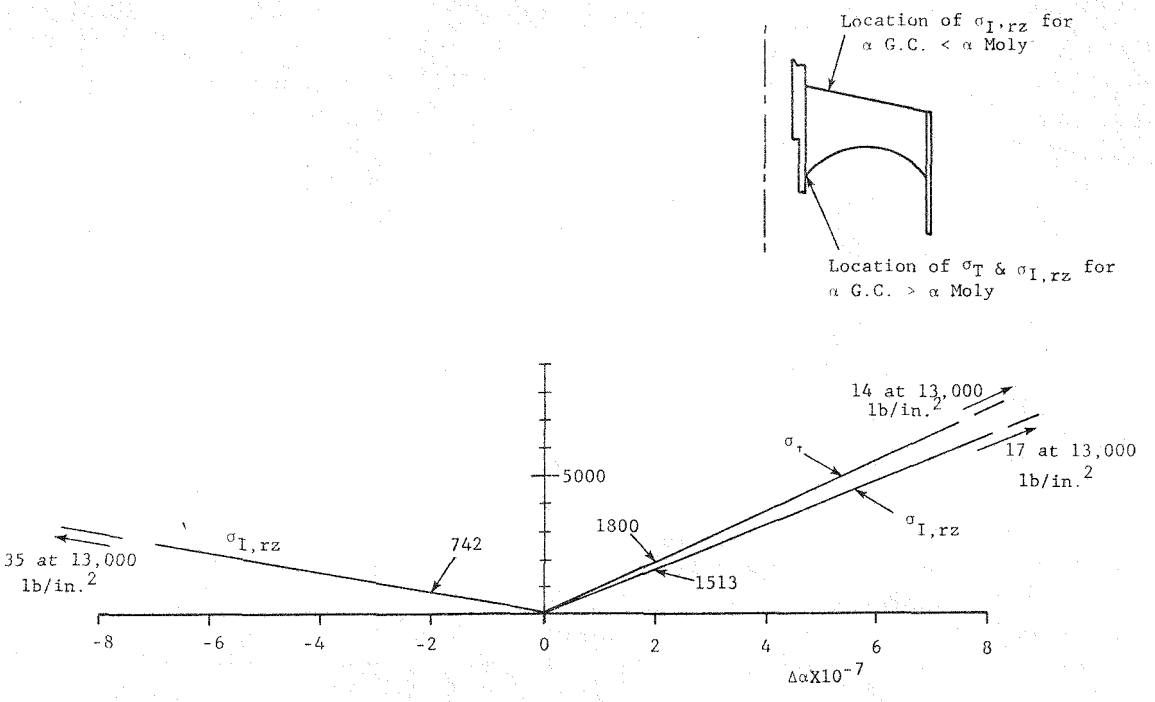

Figure 22. Extrapolation of the Maximum Principal Stresses to Highest Stress Levels. ($\sigma_{I,rz}$ for Case One and σ_T and $\sigma_{I,rz}$ for Case Two.)

The reason for the discrepancy described above is not specifically known at this time. It can be shown that for a difference in expansion of 35 x $10^{-7}/^{o}C$, tensile stresses in the molybdenum may exceed 335,000 lb/in.^{2}, which is in excess of the ultimate tensile strength. It is believed that the problem is due to the large grid size selected for this analysis and that, as the grid size decreases, stress magnitudes at regions of high stress will vary substantially.

CONCLUSIONS

For Case One, where the coefficient of expansion of the insulator was less than molybdenum, the glass-ceramic maximum principal stresses in the r-z plane at the upper surface and on most of the lower surface were tensile while the tangential stresses were entirely compressive. The principal stress of greatest magnitude (742 lb/in.^{2}) in the insulator occurred in the r-z plane on the upper surface 0.38 in. from the axis of the assembly. Another area of concern, where Zyglo adsorption has been observed at piece-part inspection, is the insulator-frame interface at the upper surface. At this location $\sigma_{I,rz}$ was 444 lb/in.^{2}.

For Case Two, where the coefficient of expansion of the glass-ceramic insulator was greater than molybdenum, the tangential stresses in the insulator were entirely tensile while the maximum principal stresses in the r-z plane were, for the most part, tensile, although a compressive region was present at the upper surface. The principal stress of greatest magnitude in the insulator (1800 lb/in.^{2}) was a tangential stress located on the lower surface near the inner sleeve.

The maximum principal stresses for both cases were not high in comparison with the ultimate tensile strength of the glass-ceramic (13,000 lb/in.^{2}). For Case One (α G.C. $<$ α molybdenum) it was found that for every 1 x $10^{-7}/^{o}C$ change in α, $\sigma_{I,rz}$ maximum increased by 371 lb/in.^{2}, while for Case Two the increase was 900 lb/in.^{2}.

According to this analysis, for the insulator to fail at 13,000 lb/in.^{2}, the expansion differences were found to be 35 and 14.4 x $10^{-7}/^{o}C$ for Cases One and Two, respectively. If the expansion difference was 35 x $10^{-7}/^{o}C$, a stress of 335,000 lb/in.^{2} in the molybdenum (greater than the ultimate strength) was predicted.

Since failures attributed to expansion mismatch have been observed in the glass-ceramic and never in the molybdenum, it is felt that residual stresses from expansion mismatch in the insulator are much higher than this analysis predicts and care should be exercised in using data generated by these means to predict the allowable expansion range prior to failure. It is believed that a smaller finite element analysis grid will show an increase in stress level at the peak stress location.

In spite of the above comment, this analysis does determine the location of the maximum stress as well as provides information concerning the general state of stress throughout the structure. The analysis will be of value in X-ray diffraction experimental stress analysis correlations.

ACKNOWLEDGMENT

The computer stress analysis was performed by M. K. Burger, Structural Analysis Division, Lawrence Livermore Laboratory, Livermore, California.

APPENDIX

FINITE ELEMENT MESH, STRESS AND STRAIN DATA

Table 1-A. Stress and Strain at the Outer Surface of the Molybdenum Frame for Case One Conditions

Axial Distance (in.)	Axial Stress ($lb/in.^2$)	Axial Strain (in./in.)	Tangential Stress ($lb/in.^2$)	Tangential Stress ($lb/in.^2$)
0.0637	0.08925	-0.0385007	9.1	-0.0384979
0.1911	0.77	-0.0385007	8.19	-0.0384986
0.3185	2.1	-0.0385	2.24	-0.0385
0.4459	3.5	-0.0384986	-15.4	-0.0385035
0.5733	3.43	-0.0384958	-52.5	-0.0385112
0.7007	-0.7	-0.0385014	-105.7	-0.0385203
0.8281	-13.3	-0.0384937	-148.4	-0.0385308
0.9555	-36.4	-0.0385014	-105.7	-0.0385203
1.0829	-69.3	-0.0385238	146.3	-0.0384636
1.21	-63.7	-0.0385665	793.8	-0.0383292
1.29	-958.3	-0.0387653	1119.3	-0.0381906
1.323	-631.4	-0.0387555	1876	-0.0380618
1.356	-238	-0.0387296	2824.5	-0.0378826
1.389	364.7	-0.0386729	3929.1	-0.0376866
1.422	1292.9	-0.0385259	4911.9	-0.0375249
1.453	4047.4	-0.0380513	6232.1	-0.0374472
1.481	4275.6	-0.0379897	6294.4	-0.0374311
1.51	4701.2	-0.0379127	6465.2	-0.0374248
1.537	5008.5	-0.0378553	6596.1	-0.0374157
1.564	5214.3	-0.0378189	6717.2	-0.0374031
1.5905	5299	-0.0378077	6816.6	-0.0373877
1.618	5248.6	-0.0378231	6890.8	-0.0373688
1.644	5033.7	-0.0378714	6930	-0.0373471
1.6707	4599.7	-0.0379631	6923	-0.0373205
1.6979	3789.1	-0.0381339	6853.7	-0.0372869
1.725	2436.1	-0.0383985	6643.7	-0.0372351

Table 2-A. Stress and Strain at the Outer Surface of the Molybdenum Frame for Case Two Conditions

Axial Distance (in.)	Axial Stress ($lb/in.^2$)	Axial Strain (in./in.)	Tangential Stress ($lb/in.^2$)	Tangential Stress ($lb/in.^2$)
0.0637	-0.07	-0.0384993	-9.1	-0.0385021
0.1911	-0.77	-0.0384993	-7.7	-0.0385014
0.3185	-2.1	-0.0385	-2.24	-0.0385
0.4459	-3.5	-0.0385014	15.4	-0.0384965
0.5733	-3.5	-0.0385042	52.5	-0.0384888
0.7007	0.91	-0.0385063	105.7	-0.0384776
0.8281	13.3	-0.0384063	148.4	-0.0384692
0.9555	36.4	-0.0384986	105.7	-0.0384797
1.0829	69.3	-0.0384762	-146.3	-0.0385364
1.21	63.7	-0.0384335	-793.8	-0.0386708
1.29	958.3	-0.0382347	-1119.3	-0.0388094
1.323	631.4	-0.0382445	-1876	-0.0389382
1.356	238	-0.0382704	-2824.5	-0.0391174
1.389	-364.7	-0.0383271	-3929.1	-0.0393134
1.422	-1292.9	-0.0384741	-4911.9	-0.0394751
1.453	-4047.4	-0.0389487	-6232.1	-0.0395528
1.481	-4275.6	-0.0390103	-6294.4	-0.0395689
1.51	-4701.2	-0.0390873	-6465.2	-0.0395752
1.537	-4980.5	-0.0391447	-6596.1	-0.0395843
1.564	-5214.3	-0.0391811	-6717.2	-0.0395969
1.5905	-5299	-0.0391923	-6816.6	-0.0396123
1.618	-5248.6	-0.0391769	-6890.8	-0.0396312
1.644	-5033.7	-0.0391286	-6930	-0.0396529
1.6707	-4599.7	-0.0390369	-6923	-0.0396795
1.6979	-3791.9	-0.0388661	-6853.7	-0.0397131
1.725	-2436.7	-0.0386015	-6643.7	-0.0397649

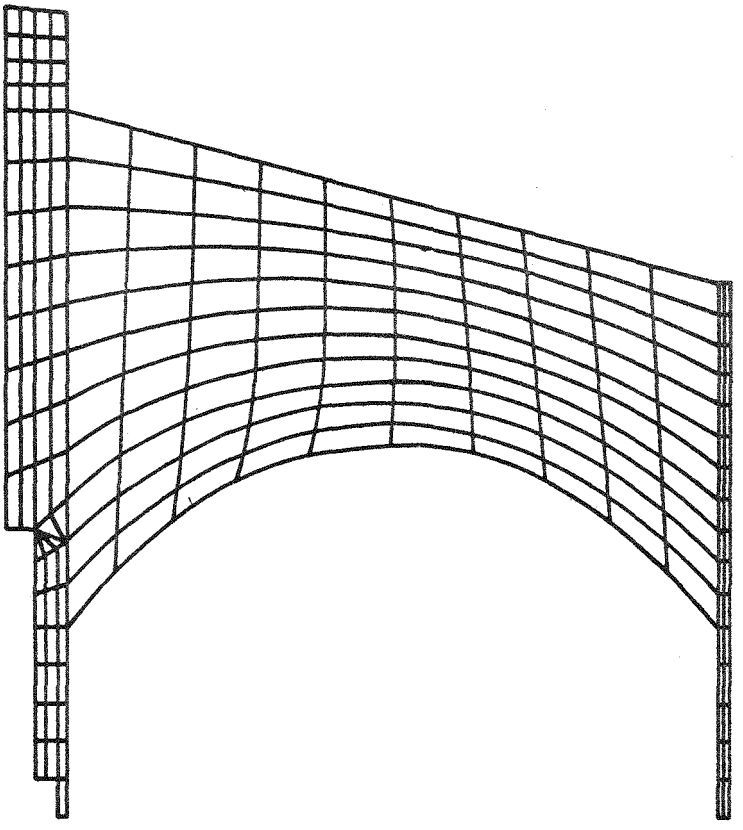

Figure 1-A. Geometry of B5N Tube Envelope Analyzed Showing Finite Element Mesh Structure

DISTRIBUTION

DOE

P. M. Ramey, PAO
TIC, Oak Ridge, (27)

GE

Technical Information Exchange
Schenectady (5)

GEND

D. H. Ahmann
R. H. Bristow
I. L. Levine
A. J. Mione
R. K. Spears
S. N. Suciu

Technical Data Library (10)
C. J. McGirr (1 Plus Reproduction Masters)

Sandia Laboratories, Albuquerque

R. R. Bassett 2354
R. J. Eagan 5845